Developmental Biology 433 (2018) 84–93

Contents lists available at ScienceDirect

Developmental Biology

journal homepage: www.elsevier.com/locate/developmentalbiology

Stk33 is required for spermatid differentiation and male fertility in mice

Leila R. Martins[a,1], Raffaela K. Bung[a,1], Stefan Koch[b,2], Karsten Richter[c], Laura Schwarzmüller[a], Dorothee Terhardt[a], Bahtiyar Kurtulmus[d], Christof Niehrs[b,e], Arefeh Rouhi[f], Ingrid Lohmann[g], Gislene Pereira[d], Stefan Fröhling[h,i,j], Hanno Glimm[h,j], Claudia Scholl[a,j,*]

[a] Division of Applied Functional Genomics, German Cancer Research Center (DKFZ) and National Center for Tumor Diseases (NCT) Heidelberg, 69120 Heidelberg, Germany
[b] Division of Molecular Embryology, DKFZ-ZMBH Alliance, 69120 Heidelberg, Germany
[c] Core Facility Electron Microscopy, DKFZ, 69120 Heidelberg, Germany
[d] Molecular Biology of Centrosomes and Cilia Unit, DKFZ-ZMBH Alliance, 69120 Heidelberg, Germany
[e] Institute of Molecular Biology (IMB), 55128 Mainz, Germany
[f] Department of Internal Medicine III, Ulm University, 89081 Ulm, Germany
[g] Department of Developmental Biology, Centre for Organismal Studies (COS), 69120 Heidelberg, Germany
[h] Division of Translational Oncology, National Center for Tumor Diseases (NCT) Heidelberg and German Cancer Research Center (DKFZ), 69120 Heidelberg, Germany
[i] Section for Personalized Oncology, Heidelberg University Hospital, 69120 Heidelberg, Germany
[j] German Cancer Consortium (DKTK), 69120 Heidelberg, Germany

ARTICLE INFO

Keywords:
Stk33
Kinase
Spermiogenesis
Spermatogenesis
Infertility
Manchette

ABSTRACT

Spermiogenesis is the final phase during sperm cell development in which round spermatids undergo dramatic morphological changes to generate spermatozoa. Here we report that the serine/threonine kinase Stk33 is essential for the differentiation of round spermatids into functional sperm cells and male fertility. Constitutive *Stk33* deletion in mice results in severely malformed and immotile spermatozoa that are particularly characterized by disordered structural tail elements. Stk33 expression first appears in primary spermatocytes, and targeted deletion of *Stk33* in these cells recapitulates the defects observed in constitutive knockout mice, confirming a germ cell-intrinsic function. Stk33 protein resides in the cytoplasm and partially co-localizes with the caudal end of the manchette, a transient structure that guides tail elongation, in elongating spermatids, and loss of Stk33 leads to the appearance of a tight, straight and elongated manchette. Together, these results identify Stk33 as an essential regulator of spermatid differentiation and male fertility.

1. Introduction

Infertility affects more than 7% of men worldwide (Agarwal et al., 2015), and in more than half of the cases the origin of the fertility defect is unknown (Punab et al., 2016). Mice represent an excellent model organism for the study of human infertility, since a great majority of the genes and processes involved in sperm production appear to be conserved between mice and men (Matzuk and Lamb, 2008). Indeed, studies using genetically modified mice resulted in several major advances in understanding the molecular basics of spermatogenesis (Cooke and Saunders, 2002). Despite this, spermatogenesis, i.e. the process of sperm cell development, remains incompletely understood.

Spermatogonia type A, which are located at the basement membrane of the seminiferous tubules, undergo mitotic divisions to maintain the male germ stem cell pool. Once committed to differentiation, spermatogonia type B give rise to primary spermatocytes, which enter meiosis. In the first meiotic cell division, meiosis I, prophase is the most time-consuming phase consisting of the leptotene, zygotene, pachytene and diplotene periods. Secondary spermatocytes that arise from meiosis I enter a second division to generate haploid round spermatids (meiosis II). During the last phase of spermatogenesis, called spermiogenesis, round spermatids undergo profound morphological changes to mature into elongated spermatids and finally spermatozoa. These changes include remodeling and removal of residual cytoplasm, acrosome formation, chromatin condensation,

* Corresponding author at: DKFZ and NCT Heidelberg, Im Neuenheimer Feld 581, 69120 Heidelberg, Germany.
E-mail address: claudia.scholl@nct-heidelberg.de (C. Scholl).
[1] Co-first authors.
[2] Present address: Department of Clinical and Experimental Medicine (IKE), Linköping University, S-58185 Linköping, Sweden.

https://doi.org/10.1016/j.ydbio.2017.11.007
Received 14 June 2017; Received in revised form 13 November 2017; Accepted 13 November 2017
Available online 16 November 2017
0012-1606/

nucleus elongation and tail development. As sperm cells differentiate, they migrate towards the lumen of the seminiferous tubules where spermatozoa are released by a process called spermiation into the caput epididymis. During their passage through the caput and corpus of the epididymis, spermatozoa undergo further maturation and acquire functional competence before being stored in the cauda of the epididymis (Borg et al., 2010; Hermo et al., 2010). Throughout spermatogenesis, somatic Sertoli cells nurture the developing sperm cells, assist in their movement towards the lumen, regulate spermiation and maintain the integrity of the seminiferous tubules (Mruk and Cheng, 2004; O'Donnell et al., 2011; Petersen and Söder, 2006).

The transition from round to elongated spermatids is aided by a transient skirt-like structure consisting of microtubules and actin filaments named manchette (O'Donnell and O'Bryan, 2014). The manchette assists in head shaping and transport of tail structural proteins to the base of the developing sperm tail. Hence, defects in manchette formation are commonly associated with disorganized sperm tail structure and head malformations (Lehti and Sironen, 2016). Despite the major role of the manchette in spermiogenesis, its assembly and disassembly, as well as the intra-manchette transport are still not well characterized.

The fully developed sperm tail can be divided into three parts according to the structural elements that surround the central axoneme. In the most proximal mid piece, mitochondria are arranged in a helix surrounding nine outer dense fibers (ODFs) and the axoneme. In the subsequent principal piece, mitochondria are absent and two ODFs are replaced by fibrous sheath (FS) longitudinal columns, which are connected to each other by circumferential ribs. In the end piece, the axoneme is solely surrounded by the plasma membrane. The different structural elements of the sperm tail are vital to the maintenance of the tail structure and motility of sperm cells (Turner, 2003).

STK33 is a serine/threonine kinase highly conserved between human and mouse (Mujica et al., 2001). It is a widely expressed gene with predominant expression in testis, ovary, lung, trachea, brain, retina, and embryonic organs (Mujica et al., 2001, 2005; Reuss et al., 2017; Scholl et al., 2009; Uhlen et al., 2015). The biochemical and biological functions of STK33 are largely unknown. There is evidence that STK33 can exert oncogenic functions in malignant tumors. Our own work demonstrates that the expression of STK33 is required for the survival of human cancer cell lines that are dependent on mutant KRAS (Azoitei et al., 2012; Scholl et al., 2009). Moreover, STK33 expression is upregulated in patients with hepatocellular carcinoma, and higher STK33 expression correlated with advanced disease stages and shorter disease-free survival (Yang et al., 2016). Despite these findings, little is known concerning the upstream regulators and downstream targets of STK33. Stk33 binds and phosphorylates the intermediate filament vimentin (Brauksiepe et al., 2008), it binds to c-Myc and increases its transcriptional activity in hepatocellular carcinoma cells (Yang et al., 2016), and it is a client of the chaperone HSP90 in human cancer cells (Azoitei et al., 2012). Notwithstanding the identification of STK33 as a possible prognostic marker and target for genotype-directed therapy in certain cancer types, its physiological function remains a mystery.

In order to gain insight into the physiological role of Stk33, we generated *Stk33* knockout mice and found that Stk33 plays a major role in mouse spermiogenesis. Stk33 loss resulted in malformation of the manchette and subsequent severely disorganized tail structures, leading to the generation of spermatozoa with abnormal immotile tails and consequently male infertility.

2. Materials and methods

2.1. Mice

Mice were housed within the DKFZ animal facility. For all mouse experiments, mice were euthanized and then further analyzed. All experiments were approved by the regional authority in Karlsruhe and performed according to federal and institutional guidelines. If not mentioned otherwise, adult Stk33 mice older than 6 weeks were used for this study. For the generation of the mouse lines and experimental details, see *Supplemental Experimental Procedures*.

2.2. Histology, IHC and IF

Histological analysis and stainings were performed by standard procedures. For IHC, anti-Stk33 (Proteintech) antibody was used in combination with Vectastain® Elite ABC Kit (AEC chromogen). The following antibodies were used for IF: anti-Stk33 (Proteintech), anti-acetylated tubulin (clone 6-11B-1, Sigma), anti-vimentin (clone 4A4, Abcam), anti-cleaved caspase3 (Cell Signaling Technologies). See *Supplemental Experimental Procedures* for details.

2.3. Western blot

Western blot analyses were performed according to standard procedures. The following antibodies were used: anti-Stk33 (Millipore), in-house produced anti-Stk33 using a previously published peptide (Mujica et al., 2005) and anti-β-actin (Clone 137CT26.1.1, Abgent). See *Supplemental Experimental Procedures* for details.

2.4. Co-immunoprecipitation

Whole testis lysates were prepared according to standard procedures. Stk33 was immunoprecipitated using anti-Stk33 (produced in-house) and SureBeadsTM Protein G Magnetic Beads (BioRad), and immobilized proteins were subjected to SDS-PAGE and Western blotting, followed by interaction partner detection with anti-α-tubulin (abcam, #18251) and Clean Blot IP Detection Kit (ThermoFisher Scientific). See *Supplemental Experimental Procedures* for details.

2.5. Transmission electron microscopy

For electron microscopy, samples were fixed in 2% glutaraldehyde, 4% formaldehyde, 100 mM NaP in PBS overnight at 4 °C. Fixed samples of seminiferous tubules and epididymal single cells were embedded in low-melting agarose and standard epoxide, followed by ultrathin sectioning. Images were taken with the Zeiss EM910 microscope and TRS CCD-Camera.

2.6. Flow cytometry

Flow cytometry was used for the analysis of cell viability, cell cycle, and identification of different cell types from testicular single cell preparations. For details see *Supplemental Experimental Procedures*.

2.7. Statistical analysis

The graphs display the mean with error bars indicating the SEM. Statistical analyses were performed with GraphPad Prism Versions 5 and 7. For details of the performed tests see *Supplemental Experimental Procedures*. Asterisks indicate the following P values: *, $P \leq 0.05$, **, $P \leq 0.01$, ***, $P \leq 0.001$, ****, $P \leq 0.0001$.

3. Results

3.1. Characteristics of Stk33 knockout mice

To investigate the physiological function of the uncharacterized serine/threonine kinase Stk33, we generated constitutive *Stk33* knockout mice (Stk33.KO) by crossing floxed *Stk33* mice (Stk33.lox) with a CMV-cre deleter strain (Fig. 1A). The subsequent deletion of exon 7 removes part of the Stk33 kinase domain and leads to a frameshift

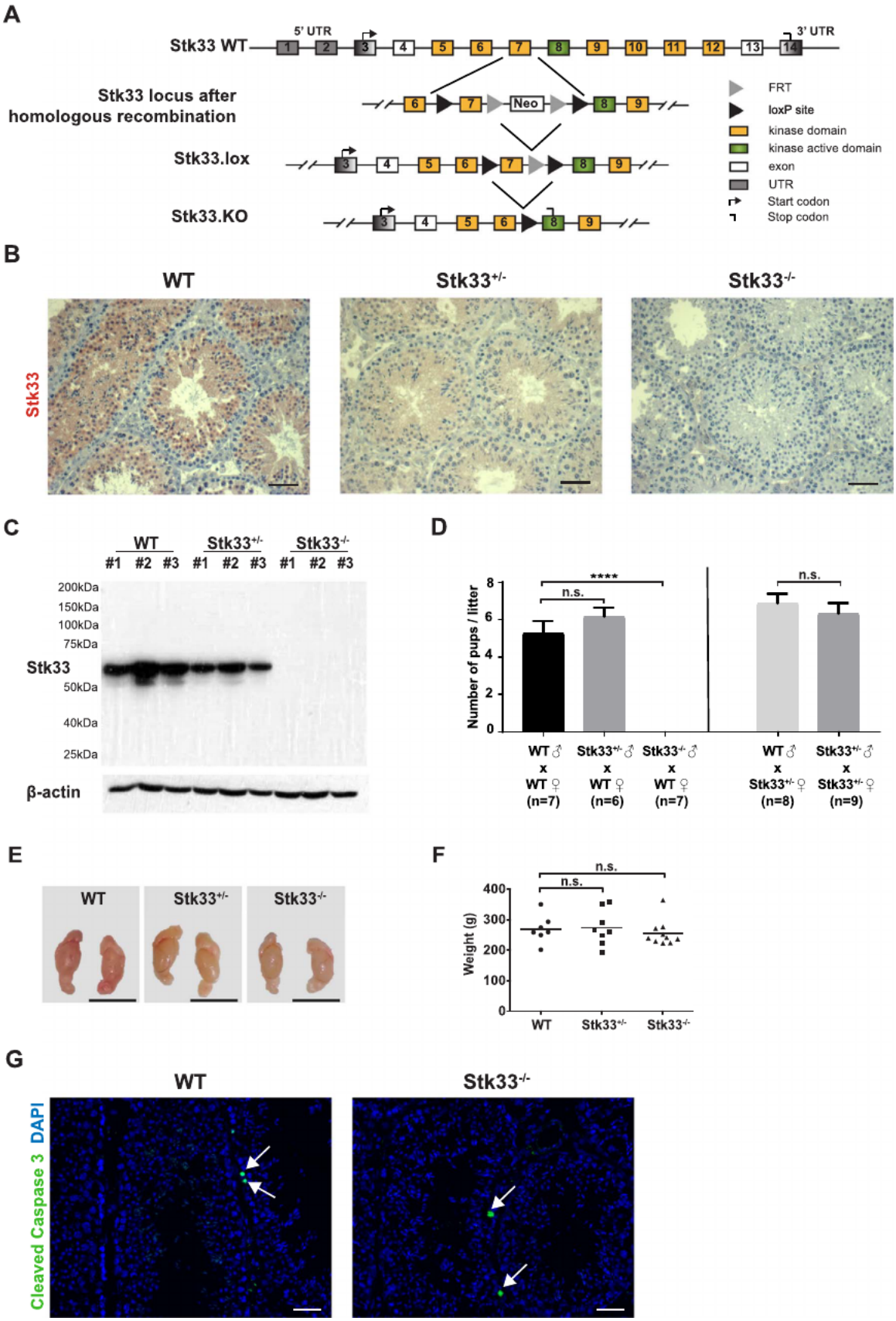

Fig. 1. Stk33 deletion leads to male infertility in mice. (A) Strategy for generating conditional and germline *Stk33* knockout mice. UTR, untranslated region; FRT, flippase recognition target site; neo, neomycin resistance gene. (B) IHC staining of Stk33 in seminiferous tubules of WT, Stk33$^{+/-}$ and Stk33$^{-/-}$ mice. Scale bar, 50 μm. (C) Western Blot of testes from WT, Stk33$^{+/-}$, and Stk33$^{-/-}$ mice (n = 3 per genotype) using anti-Stk33 (Millipore) and anti-β-actin antibodies. (D) Litter size in the indicated crossing combinations. n.s., not significant. (E) Representative images of testes from WT, Stk33$^{+/-}$ and Stk33$^{-/-}$ mice. Scale bar, 1 cm. (F) Weight of testes and epididymides from WT, Stk33$^{+/-}$ and Stk33$^{-/-}$ mice. n.s.: not significant. (G) IF staining of cleaved Caspase 3 indicating apoptotic cells in the testis of WT and Stk33$^{-/-}$ mice. Arrows point to positive cells. Scale bar, 40 μm.

resulting in a premature stop codon at the second amino acid in exon 8. Homozygous Stk33.KO ($Stk33^{-/-}$) mice that originated from heterozygous Stk33.KO ($Stk33^{+/-}$) matings were obtained at normal Mendelian ratios. Adult $Stk33^{-/-}$ mice appeared normal, and full necropsy of several adult mice (male, n = 6; female, n = 5) revealed no macroscopic differences compared to wildtype (WT) or $Stk33^{+/-}$ littermates (data not shown). To validate successful Stk33 deletion, we examined the presence of Stk33 protein in testis, lung, and ovary, which are characterized by high physiologic Stk33 mRNA expression (Fig. S1A). We confirmed lack of Stk33 protein in testis of $Stk33^{-/-}$ mice by immunohistochemistry (IHC) and Western blot (Fig. 1B, C and S1B). However, Stk33 protein could still be detected in the ciliated epithelium of lung and oviduct (Fig. S1C). By performing a series of reverse transcription PCRs with primers binding in different exons of *Stk33* and sequencing of the PCR products, we revealed that skipping of exon 8 resulted in the expression of an in-frame *Stk33* mRNA lacking exon 7 and exon 8 in ovary and lung (Fig. S1D and S1E and data not shown). This enables the translation of a shortened Stk33 protein that lost 76 amino acids of the kinase domain including the active site. Importantly, exon 8 skipping was not observed in testis, where we could amplify the predicted mRNA lacking exon 7, leading to a frame-shift and full loss of Stk33 protein (Fig. S1D and S1E). Based on these results, we assume that the $Stk33^{-/-}$ mice might express kinase-dead Stk33 protein in the whole organism with the exception of testis, suggesting that the catalytic activity of Stk33 may be dispensable for mouse development, considering the absence of an obvious phenotype.

3.2. Targeted disruption of Stk33 results in male infertility

Given the high physiological Stk33 expression in testis and its successful depletion in this tissue, we decided to analyze the fertility of $Stk33^{+/-}$ and $Stk33^{-/-}$ mice by controlled breeding experiments. Despite normal reproductive behavior and production of copulatory plugs, $Stk33^{-/-}$ males were unable to produce offspring when crossed with WT females (Fig. 1D and S1F). In contrast, $Stk33^{+/-}$ males were fertile to the same extend as WT males, as indicated by the time spent to generate offspring and the number of pups per litter (Fig. 1D and S1F). Macroscopic evaluation of testis and epididymis revealed no difference in morphology, size or weight among WT, $Stk33^{+/-}$ and $Stk33^{-/-}$ mice (Fig. 1E and F), and we could not detect any changes in the viability of testicular cells lacking Stk33 (Fig. 1G), suggesting that the infertility of male $Stk33^{-/-}$ mice is due to a functional defect of sperm cells.

3.3. Loss of Stk33 results in severe morphological tail aberrations in spermatozoa

In order to determine the cause for the inability to produce offspring, we investigated the morphology of testicular and epididymal cells of Stk33 deficient mice. Analysis of the DNA content by flow cytometry of DAPI stained single cell preparations did not show any difference in the population distribution of testicular cells lacking Stk33, suggesting that Stk33 does not influence the turnover of diploid cells or the generation of haploid cells during the first part of spermatogenesis (Fig. 2A). Accordingly, flow cytometry analysis of testicular cells stained with Hoechst 33342 (Bastos et al., 2005) showed that WT and $Stk33^{-/-}$ mice presented a similar distribution of the different sperm cell types from spermatogonia to elongated spermatids (Fig. 2B and S2A). Histological examination of seminiferous tubules confirmed that all cell types until elongating spermatids could be observed in the testis of $Stk33^{-/-}$ mice (Fig. 2C). However, the long tails of spermatozoa were completely absent in the lumen of the seminiferous tubules of $Stk33^{-/-}$ mice, suggesting a role for Stk33 in the differentiation of spermatozoa during spermiogenesis (Fig. 2C). The absence of fully developed tails could also be appreciated by immunofluorescence using an anti-acetylated tubulin antibody that specifically stains the flagellum (Fig. 2D). Consistent with this finding, the number of spermatozoa with a tail-like structure was significantly reduced in single cell preparations of testes (Fig. 2E) as well as epididymides from $Stk33^{-/-}$ mice (Fig. 2F). In contrast to cells isolated from the cauda epididymis of WT and $Stk33^{+/-}$ mice, we were not able to identify a single $Stk33^{-/-}$ spermatozoon that displayed motility (Fig. 2G). Hematoxylin staining of these cells revealed short, often coiled and abnormally shaped tails (Fig. 2H). Histological analysis of the cauda epididymis in $Stk33^{-/-}$ mice showed the accumulation of cellular debris rather than normally developed spermatozoa (Fig. 2I).

In order to characterize the morphological alterations in more detail, we analyzed the structure of spermatozoa isolated from the epididymis by transmission electron microscopy (TEM). We observed only few spermatozoa or sperm heads in $Stk33^{-/-}$ compared to WT mice, where many sections of straight flagella representing regular morphology from mid- to end-piece could be seen (Fig. S2B and 2J). In line with the results obtained by light microscopy, we could not detect a single perfectly organized sperm tail in the epididymis of $Stk33^{-/-}$ mice. $Stk33^{-/-}$ spermatozoa exhibited defects such as head-dislocation and particularly a lack of tail organization (Fig. 2K). Although all structural elements were present in most spermatozoa, FS proteins segregated in accumulation bodies without forming ribs or longitudinal columns, ODFs were disorganized, and mitochondria did not align in the characteristic helix shape around the mid piece (Fig. 2K and L). Collectively, the observed malformations caused by Stk33 loss contribute to the inability of spermatozoa to form a functional tail, leading to infertility of $Stk33^{-/-}$ males.

3.4. Infertility associated with Stk33 loss is germ cell speci c

Spermiogenesis defects may be germ cell-intrinsic, or result from defective interaction of spermatids with their supporting cells in the testis, particularly Sertoli cells. Brauksiepe and colleagues reported that Stk33 phosphorylates vimentin *in vitro,* and that Stk33 and vimentin form a complex in a Sertoli cell line (Brauksiepe et al., 2008). Since aberrant distribution of vimentin filaments in Sertoli cells was previously associated with altered spermatogenesis (Alam and Kurohmaru, 2014; Hall et al., 1991; Johnson, 2014; Kleymenova et al., 2005), we hypothesized that Stk33 loss could interfere with cytoskeleton organization in Sertoli cells and/or Sertoli-germ cell interactions, leading to a failure in spermatogenesis. However, the expression of vimentin in Sertoli cells of $Stk33^{-/-}$ and WT mice was comparable, presenting the characteristic basal perinuclear distribution and the stage-specific apical expression (W Chung et al., 2010) (Fig. 3A). Unaltered vimentin expression and distribution, along with maintenance of Sertoli cell morphology, suggested that Stk33 deletion might not affect Sertoli cells but rather germ cells directly, which is supported by our finding that Stk33 is not expressed in Sertoli cells (see below). To further test this hypothesis, we crossed the conditional Stk33.lox mice with a mouse strain expressing Cre recombinase under control of the Stra8 promoter (Stra8-Cre) (Anderson et al., 2008). Stk33.lox/Stra8-Cre mice express Cre recombinase in preleptotene spermatocytes, which deletes Stk33 specifically in immature germ cells. Efficient Cre recombination and consequent loss of Stk33 expression in the testis was confirmed by Western blot analysis (Fig. 3B). Stk33 deletion in germ cells significantly decreased the number of sperm cells with tail-like structures in testis (Fig. 3C) and epididymis (Fig. 3D). Moreover, spermatozoa harvested from the epididymis were immotile and exhibited severe tail malformations similar to the ones observed in $Stk33^{-/-}$ mice (Fig. 3E and F). Occasionally, spermatozoa with normal morphology and motility could be found in the epididymis of Stk33.lox/Stra8-Cre mice, which is most likely due to incomplete Cre recombination in some cells. Overall, the phenotype observed in Stk33.lox/Stra8-Cre mice recapitulated the defects in $Stk33^{-/-}$ mice, verifying that *Stk33* knockout-associated infertility is germ cell specific, and suggesting that Stk33 expression is essential for sperm maturation after the onset of meiosis.

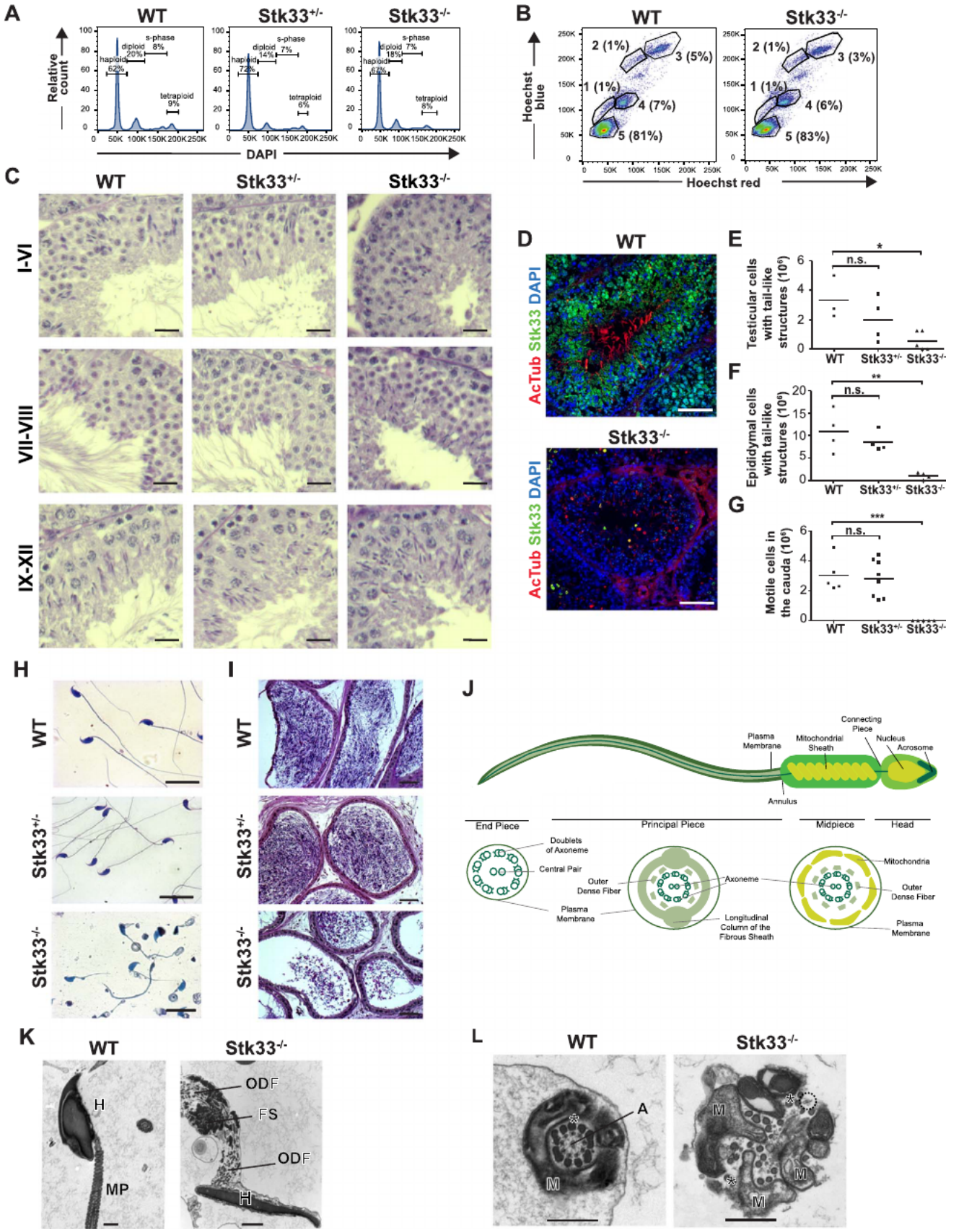

Fig. 2. Stk33 loss leads to severe malformations in spermatozoa. (A) DNA content analysis of single cells from testes of WT, Stk33$^{+/-}$ and Stk33$^{-/-}$ mice to identify cells at different phases during meiotic and mitotic cell divisions. Cells were stained with DAPI and analyzed by flow cytometry. (B) Flow cytometry of Hoechst stained single cells from testes of WT and Stk33$^{-/-}$ mice that allow the discrimination of spermatogonia (1), preleptotene spermatocytes (2), spermatocytes I (3), spermatocytes II (4), and round and elongated spermatids (5). (C) Periodic acid-Schiff (PAS) staining of testis sections showing stages I-VI, VII-VIII and IX-XII of spermatogenesis in the seminiferous tubules of WT, Stk33$^{+/-}$ and Stk33$^{-/-}$ mice. Scale

bar, 20 µm. (D) IF staining of seminiferous tubules from WT and Stk33$^{-/-}$ mice with anti-Stk33 (Proteintech), anti-acetylated tubulin (AcTub), and DAPI for nuclear staining. Scale bar, 50 µm. (E, F) Number of cells with tail-like structures in single cell preparations from testes (E) and epididymides (F) of WT, Stk33$^{+/-}$ and Stk33$^{-/-}$ mice. n.s.: not significant. (G) Number of motile cells in the cauda epididymidis of WT, Stk33$^{+/-}$ and Stk33$^{-/-}$ mice. n.s.: not significant. (H) H & E staining of spermatozoa isolated from epididymides of WT, Stk33$^{+/-}$, and Stk33$^{-/-}$ mice. Scale bar, 20 µm. (I) H & E staining of cauda epididymidis sections from WT, Stk33$^{+/-}$, and Stk33$^{-/-}$ mice. Scale bar, 50 µm. (J) Schematic drawing of a spermatozoon. The different structures of the tail are depicted below as cross-sections (adapted from Borg et al. (2010)). (K, L) TEM images of spermatozoa from epididymides of WT and St33$^{-/-}$ mice displayed as longitudinal sections (K, scale bar, 1 µm) and cross-sections of the tail midpiece (L, scale bar, 0.5 µm). H, head; MP, midpiece; ODF, outer dense fibers; FS, fibrous sheath; A, axoneme; M, mitochondria; asterisk, outer dense fibers; dotted circle, microtubule.

3.5. Stk33 expression is initiated during meiosis I

In order to better understand at which period during development of spermatozoa Stk33 loss has an impact on sperm cell differentiation, we sought to evaluate Stk33 expression in different sperm cell types by analyzing testes from newborn WT mice undergoing the first round of spermatogenesis. In these mice, the appearance of sperm cells in the seminiferous tubules is synchronized, and the exact time point each cell type arises for the first time is well defined (Fig. 4A) (Bellvé et al., 1977; Nebel et al., 1961). As shown by Western blot analysis, Stk33 was absent at day 6 postpartum (P6) when only spermatogonia A and Sertoli cells are present, and continued to be negative until P10 with appearance of the leptotene period of meiosis I (Fig. 4B). At P18, when all cell types until secondary spermatocytes are present, we observed a substantial increase in Stk33 expression, suggesting that Stk33 is up-regulated during meiosis I after leptotene period (Fig. 4B). A similar

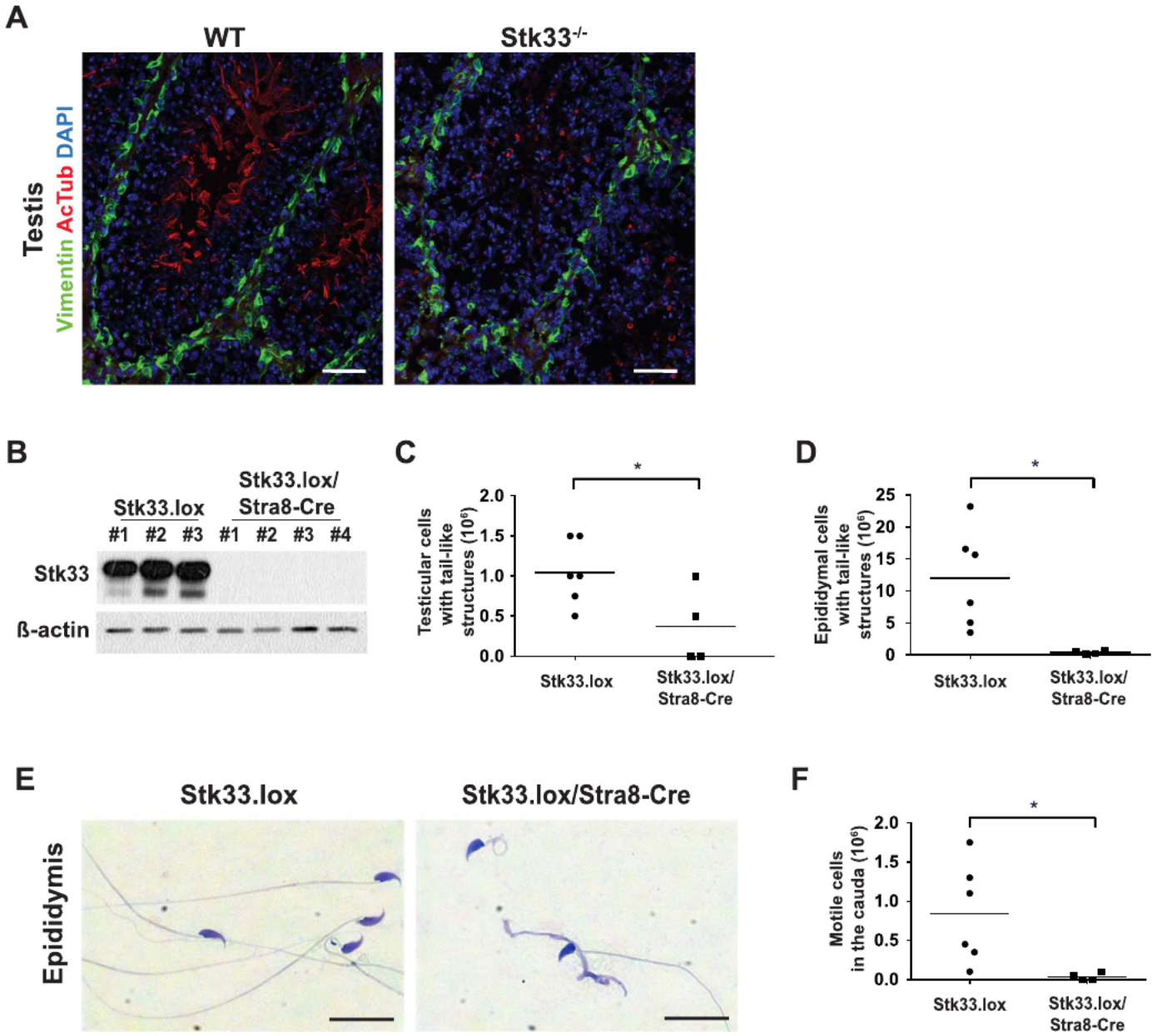

Fig. 3. Stk33 knockout-induced phenotype is germ cell specific. (A) IF staining of seminiferous tubules from WT and Stk33$^{-/-}$ mice with anti-vimentin, anti-acetylated tubulin (AcTub), and DAPI for nuclear staining. Scale bar, 50 µm. (B) Western Blot of testes from 3 Stk33.lox and 4 Stk33.lox/Stra8-Cre mice using anti-Stk33 (produced in-house) and anti-β-actin. (C, D) Number of cells with tail-like structures in single cell preparations from testes (C) and epididymides (D) of Stk33.lox and Stk33.lox/Stra8-Cre mice. (E) H & E staining of spermatozoa isolated from epididymides of Stk33.lox and Stk33.lox/Stra8-Cre mice. Scale bar, 20 µm. (F) Number of motile cells in the cauda epididymidis of Stk33.lox and Stk33.lox/Stra8-Cre mice.

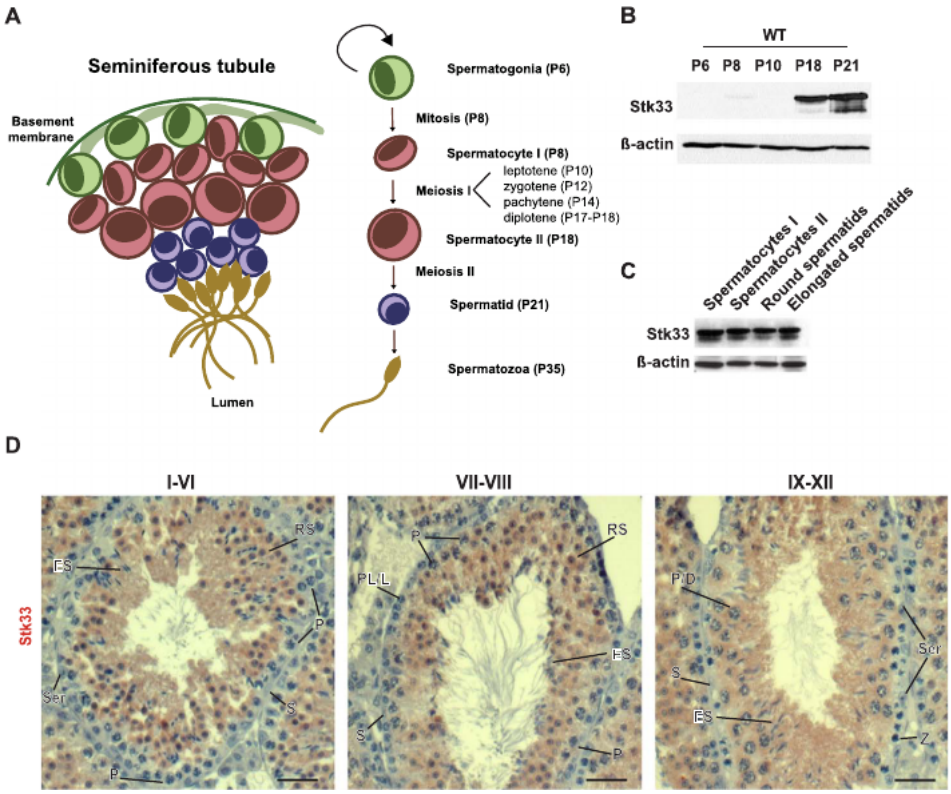

Fig. 4. Stk33 is expressed in meiotic and post meiotic sperm cells. (A) Schematic drawing of a cross-section of a seminiferous tubule (left) and the different cell types during spermatogenesis (right). P6 to P35 indicates the postnatal day, at which the respective cell type can be first detected in testes. (B) Western Blot of testes from WT mice resected at the indicated time points after birth using anti-Stk33 (produced in-house) and anti-β-actin. P, postnatal. (C) Western Blot of FACS-sorted cells from testes of adult WT mice using anti-Stk33 (Millipore) and anti-β-actin. (D) IHC staining with anti-Stk33 (Proteintech) of seminiferous tubules of WT mice displaying Stk33 expression in different stages of spermatogenesis. S, spermatogonia; P, pachytene spermatid; P/D, pachytene/diplotene spermatocyte; PL/L, pre-leptotene/leptotene spermatocyte; Z, zygotene spermatocyte; ES, elongated spermatid; RS, round spermatid; Ser, sertoli cell. Scale bar, 30 µm.

expression pattern was observed in published mRNA expression profiles from testes at different time points after birth, and the same data also demonstrated the absence of *Stk33* expression in Sertoli and interstitial cells (Fig. S2C) (Schultz et al., 2003). Isolation of different sperm cell types from testes of adult mice using Hoechst 33342 staining (Fig. 2B and S2A) and fluorescence-activated cell sorting (FACS) followed by Western blot analysis demonstrated high levels of Stk33 protein expression already in primary spermatocytes, confirming that Stk33 expression increases during meiosis I (Fig. 4C). In line with this, IHC analysis of seminiferous tubules revealed an increase in Stk33 expression in pachytene spermatocytes (primary spermatocytes in prophase I) from stage I-VI to stage VII-VIII, while spermatogonia, leptotene and zygotene spermatocytes showed low to absent levels of Stk33 (Fig. 4D). High levels of Stk33 protein expression are maintained after meiosis I and II in spermatids as shown by IHC (Fig. 4D), Western blot analysis of sorted populations (Fig. 4C), and total cells present in the testis of mice at P21 (Fig. 4B). Together, these observations indicate that Stk33 expression is initiated in primary spermatocytes in meiosis I during the pachytene period, and is maintained during spermatogenesis.

3.6. *Stk33 expression is essential for correct manchette function*

To gain insight into the mechanism by which Stk33 regulates spermiogenesis, we analyzed the different steps of spermatid differentiation in the testis of Stk33$^{-/-}$ mice by TEM. Early phases of acrosome formation in round spermatids appeared unaffected by Stk33 deletion, as we observed correct formation of the acrosomal vesicle, shaping of the acrosomal cap and differentiation of the acroplaxome (Fig. 5A). Nonetheless, during nucleus elongation and acrosome shaping, elongating spermatids developed several acrosomal and head malformations, such as oversized acrosomal tips and bifurcated heads (Fig. 5B). The initial development of the core of the flagellum, the axoneme, also seemed to be unperturbed in Stk33$^{-/-}$ testis, since long stretches of the typical 9 × 2 + 2 microtubule structure could be observed in early steps (Fig. 5C). However, at later steps, the organization of the axoneme was lost and the delivery and/or assembling of the accessory tail components appeared to be compromised in Stk33$^{-/-}$ spermatids, as unorganized ODF and FS proteins were found together with unaligned, isolated microtubules (Figs. 2L and 5C). Finally, intercalation of mitochondria between the neck and annulus in late spermiogenesis did not take place in Stk33$^{-/-}$ elongating spermatids, evident by the lack of an organized mid piece (Fig. 2K and L).

The presence of malformed heads and disorganized tail structures suggested that defects in formation and/or function of the manchette could be the underlying reason for the observed phenotype in Stk33$^{-/-}$ spermatids. Therefore, we sought to analyze the organization of this transient structure in WT and Stk33$^{-/-}$ spermatids in more detail by TEM and IF staining of the manchette microtubules with an anti-acetylated tubulin antibody. As shown in Fig. 5D, E and S3, the manchettes in Stk33$^{-/-}$ spermatids were abnormally elongated and straight, and lacked the basket-like distal termination. This phenotype could be caused by a delayed manchette removal and/or impaired movement, or indirectly through malfunction of intra-manchette transport. Investigation of the manchette at different steps during spermatid elongation using IF suggests that the early manchette formation seems to be intact, and disintegration of the manchette took place (Fig. 5E). It is possible that the manchette movement/function, which is normally involved in shaping of the distal half of the sperm head, is disturbed in Stk33$^{-/-}$ mice, resulting in an abnormally elongated head of Stk33$^{-/-}$ spermatids (Fig. S3). In line with these

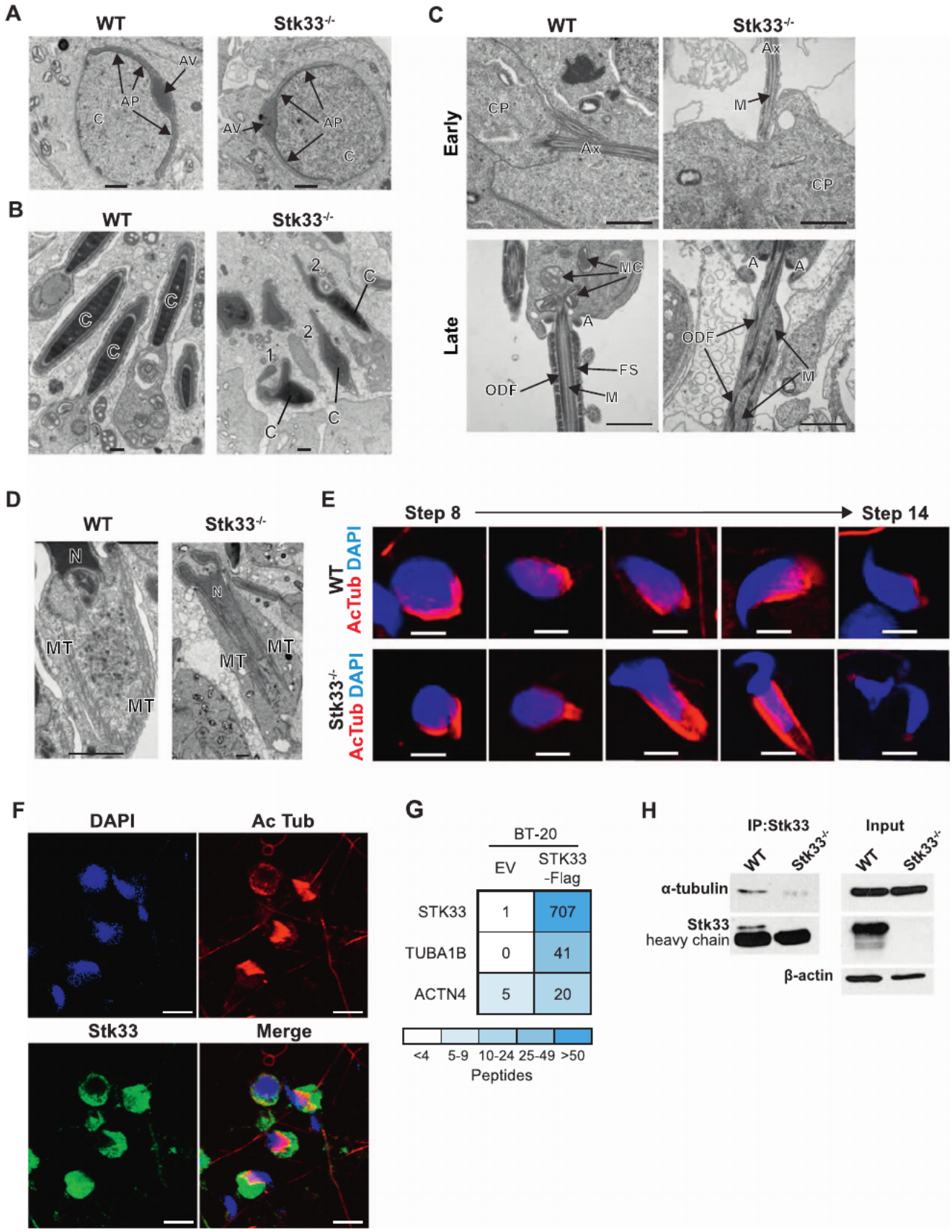

Fig. 5. Stk33 loss results in manchette malformation. (A) TEM images of round spermatids in testes from WT and Stk33$^{-/-}$ mice. AP, acroplaxome; AV, acrosomal vesicle; C, chromatin. Scale bar, 1 μm. (B) TEM images of spermatozoa in testes from WT and Stk33$^{-/-}$ mice displaying heads with already condensed chromatin and acrosome formation. 1, bifurcated head; 2, oversized tip; C, chromatin. Scale bar, 1 μm. (C) TEM images of testes from WT and Stk33$^{-/-}$ mice showing flagella organization at early and late steps of spermatid differentiation. A, annulus; Ax, axoneme; CP, cytoplasm; FS, fibrous sheath; M, microtubule; MC, mitochondria; ODF, outer dense fibers. Scale bar, 1 μm. (D) TEM image of the manchette of an elongating spermatid in the testis of WT and Stk33$^{-/-}$ mice. MT, manchette microtubule; N, nucleus. Scale bar, 1 μm. (E) IF staining of manchette formation in elongating spermatids

from WT and Stk33$^{-/-}$ mice using anti-acetylated Tubulin (AcTub) and DAPI for nuclear staining. Exemplary images of spermatids from step 8 to step 14 are shown. Scale bar, 5 μm. (F) IF staining of cells isolated from testes of WT mice using anti-Stk33 (Proteintech), anti-acetylated tubulin (AcTub), and DAPI for nuclear staining. The merged picture shows co-localization of Stk33 and the caudal end of the manchette in elongating spermatids (yellow color). Scale bar, 10 μm. (G) Number of peptides representing the indicated proteins detected by mass spectrometry after immunoprecipitation with an anti-Flag antibody from BT-20 cells stably transduced with either empty vector (EV) or Flag-tagged Stk33. (H) Immunoprecipitation (IP) of Stk33 (produced in-house) from WT and Stk33$^{-/-}$ whole testis lysates, followed by detection with the indicated antibodies demonstrating binding of Stk33 to α-tubulin. Input and β-actin controls are shown on the right.

results, we detected Stk33 protein in the cytoplasm, co-localizing with the caudal end of the manchette in elongating spermatids, suggesting that Stk33 binds directly to the manchette filaments and plays a critical role in manchette organization and function (Fig. 5F). In support of this observation, our previous proteomics analysis of STK33 interaction partners in the breast cancer cell line BT-20 identified cytoskeletal proteins (Azoitei et al., 2012). Specifically, we found the alpha-tubulin TUBA1B and the alpha-actin ACTN4 to be co-immunoprecipitated with Flag-tagged STK33 (Fig. 5G). To validate these results, we immunoprecipitated Stk33 from testis protein lysates, and detected α-tubulin in the sample from WT mice but not from Stk33$^{-/-}$ mice (Fig. 5H). Collectively, these findings suggest that Stk33 might regulate microtubule organization and/or activity essential for manchette function, thereby influencing the proper formation of spermatozoa.

4. Discussion

STK33 is a serine/threonine kinase that has been implicated in tumorigenesis (Scholl et al., 2009; Yang et al., 2016), however its exact function as well as upstream regulators and downstream effectors in normal physiology and malignant disease are unknown. In this study, we show, by using a genetically engineered knockout mouse model, that Stk33 is a vital component for spermiogenesis and male fertility. Loss of Stk33 leads to abnormal head shaping and severe impairment of tail development in spermatozoa, which was associated with defects in manchette function.

Stk33 expression in mice and men is the highest in testis, lung, ovary and brain (this work and Scholl et al., 2009) with testis surpassing the three other organs by more than 100-fold. These organs have the unifying feature of possessing epithelia that contain cells with multiple motile cilia, or in the case of testis, sperm cells with one specialized, elongated motile cilium (Fliegauf et al., 2007), which might point to a functional role of Stk33 in ciliated cells. In support of this, Stk33 protein was detected in the ependymal cells of the brain (Reuss et al., 2017), and our studies identified Stk33 protein in the ciliated epithelium of the lung and oviduct, and in spermatocytes. The generated *Stk33* knockout mouse showed loss of Stk33 in testis, which enabled us to study the biological role of this uncharacterized serine/threonine kinase in spermatogenesis. However, the mice retained expression of a shortened Stk33 protein in lung and ovary and maybe other organs. Since this truncated protein lost critical domains within the kinase domain, the catalytic activity of Stk33 seems not to be critical for normal tissue homeostasis at least in lung and ovary, as we did not observe any obvious abnormality in these organs.

Stk33 starts to be expressed in primary spermatocytes during meiosis I and is thereafter present at all phases during sperm cell development. This expression pattern is typical for genes that are required during late phases of spermatid differentiation since they need to be transcribed in round spermatids at the latest before the onset of nuclear condensation, which comes along with transcription termination (Yan, 2009). In line with this, the testis weight and the number of viable testicular cells in Stk33$^{-/-}$ mice were unaffected, which is often seen in mice lacking genes essential for later differentiation phases, since defective spermatocytes after step 9 of spermiogenesis are no longer removed as opposed to damaged round spermatids in earlier phases (Yan, 2009). In addition, loss of Stk33 does not seem to affect meiosis and the generation of haploid round spermatids, which appeared morphologically normal with a properly positioned acrosome. However, elongated spermatids presented with disorganized flagella containing scrambled tail components, explaining the observed complete immobility of epididymal spermatozoa and consequently infertility. In addition to this most striking abnormality, some spermatids possessed head alterations in seminiferous tubules, while chromatin condensation seemed to be unaffected. These observations add Stk33 to the group of genes that are mandatory for proper spermatid differentiation, although the phenotypic changes of the corresponding knockout mice compared to the Stk33$^{-/-}$ mice are not identical. Among the KO mouse models that show impaired spermiogenesis, Kif3a (Lehti et al., 2013), Lrguk1 (Liu et al., 2015) and Spef2 (Sironen et al., 2010) present the most similar phenotype to Stk33$^{-/-}$ sperm cells. While Kif3a and Spef2 are thought to play a crucial role in microtubule-based transport, Lrguk1 seems to be essential for microtubule organization. Just like in Stk33$^{-/-}$ mice, loss of these proteins resulted in male infertility due to the generation of scarce and abnormally shaped spermatozoa, and the defects were first evident in spermatids.

It has previously been described that the intermediate filament vimentin is a physiological target of Stk33 (Brauksiepe et al., 2008), and altered vimentin in Sertoli cells is associated with defects in spermatogenesis (Alam and Kurohmaru, 2014; Hall et al., 1991; Johnson, 2014; Kleymenova et al., 2005). This suggested to us that the observed abnormalities in Stk33$^{-/-}$ testes might be caused by disturbed cytoskeleton organization in Sertoli cells. However, Stk33 was not expressed in Sertoli cells of WT mice, and accordingly, their morphology in Stk33$^{-/-}$ mice was unaffected. Furthermore, we could clearly allocate the function of Stk33 to germ cells, since the specific depletion of Stk33 in spermatocytes driven by the germ cell-specific Stra8 promoter revealed the same results as with Stk33$^{-/-}$ mice.

The simultaneous occurrence of sperm head and tail defects at late phases of spermiogenesis in genetically modified mice is often caused by a disturbed function and/or formation of the manchette, which is a temporary structure only present during spermatid elongation. The basket-like manchette is composed of microtubules and actin filaments that aid in protein transport to the flagellum during tail development, and supports nuclear elongation by moving distally while its perinuclear ring constricts the nucleus (Cole et al., 1988). Stk33$^{-/-}$ spermatids presented an irregularly elongated and straight manchette that was also observed in the KO mouse models for Kif3a (Lehti et al., 2013), Lrguk1 (Liu et al., 2015), Spef2 (Sironen et al., 2010), as well as other murine models of defective spermatid differentiation (Lehti and Sironen, 2016). In contrast to the above mouse models, stretches of well-arranged axonemes could be seen in Stk33$^{-/-}$ testis indicating that the axoneme microtubules are properly nucleated from the basal body and that the axoneme starts to elongate regularly. Nonetheless, a well-organized axoneme or properly assembled ODF or FS proteins were never observed at later steps. This might point to a role of Stk33 in intra-manchette transport and/or assembly of sperm tail secondary structures. Another possible role of Stk33 during spermiogenesis might be the stabilization of the axoneme. However, if loss of Stk33 disturbs axoneme formation at later steps, leads to axoneme disintegration or affects intra-flagellar and/or intra-manchette transport, needs to be clarified in additional studies. Further evidence that Stk33 might directly influence the structure of manchette filaments came from the observation that Stk33 is partially co-localized with the caudal end of the manchette. The exact mechanism of manchette formation is still not fully understood, but the current most favored hypothesis is that the formation of the manchette microtubules starts at the centrosome thereby establishing the plus-end towards the nucleus, and the minus-end towards the tail (Lehti and Sironen, 2016). The finding that Stk33

binds to alpha-tubulin, which is always exposed at the minus-end of microtubular structures, supports the idea that Stk33 directly interacts with the manchette.

Overall, this study identifies Stk33 as an essential player in spermatid differentiation and function. We show that loss of Stk33 in germ cells induces a failure in later phases of spermiogenesis characterized by abnormal manchette function that leads to misshaped heads and severely malformed tails of spermatozoa and, ultimately, male infertility. Stk33 protein directly interacts with alpha-tubulin, suggesting a regulatory role in microtubule organization and/or function of the manchette, which has to be tested in future studies. Expression of Stk33 in other tissues possessing ciliated epithelia could point to a general role of Stk33 in ciliated cells.

Acknowledgements

We thank Ulrike Engel from the Heidelberg University Nikon Imaging Center, Franciscus van der Hoeven from the DKFZ Transgenic Core Facility, Damir Krunic from the DKFZ Light Microscopy Core Facility, Michelle Neßling from the DKFZ Core Facility Electron Microscopy, and Klaus Hexel from the DKFZ Flow Cytometry Core Facility for valuable technical assistance and discussions, Ilse Hofmann and Claudia Tessmer from the Antibody Unit of the DKFZ Genomics and Proteomics Core Facility for Stk33 antibody generation, Alexandra Buse for technical assistance, James Horner (current address: University of Texas M.D. Anderson Cancer Center, Houston, Texas) and the Dana-Farber Cancer Institute Transgenic and Gene Targeting Core Facility for generating the Stk33.lox mice, and D. Gary Gilliland for providing the Stk33.lox mice. This study was supported by the German Research Foundation (DFG) grant SFB873 to I.L., G.P., C.N., H.G. and C.S. and DFG grant SCHO1215/2-1 to C.S.. R.K.B. was supported by a stipend from the DKFZ International Graduate School for Cancer Research.

Author contributions

C.S. designed the study and supervised the work; S.F. and H.G. co-supervised the study; I.L. and G.P. contributed to study strategy and technical aspects; L.R.M. and R.K.B. performed most experiments; A.R. performed initial macroscopic and histological analyses of Stk33.KO mice; L.S., D.T. and B.K. performed selected tissue stainings; S.K. provided essential reagents and expertise; K.R. performed transmission electron microscopy analyses; C.N. and S.K. provided the Stra8-Cre mouse strain; L.R.M., R.K.B. and C.S. wrote the manuscript with input from other authors.Conflict of interest

The authors have no conflict of interest to declare.

Appendix A. Supporting information

Supplementary data associated with this article can be found in the online version at doi:10.1016/j.ydbio.2017.11.007.

References

Agarwal, A., Mulgund, A., Hamada, A., Chyatte, M.R., 2015. A unique view on male infertility around the globe. Reprod. Biol. Endocrinol. 13, 37.
Alam, M.S., Kurohmaru, M., 2014. Disruption of Sertoli cell vimentin filaments in prepubertal rats: an acute effect of butylparaben in vivo and in vitro. Acta Histochem. 116, 682–687.
Anderson, E.L., Baltus, A.E., Roepers-Gajadien, H.L., Hassold, T.J., de Rooij, D.G., van Pelt, A.M.M., Page, D.C., 2008. Stra8 and its inducer, retinoic acid, regulate meiotic initiation in both spermatogenesis and oogenesis in mice. Proc. Natl. Acad. Sci. USA 105, 14976–14980.
Azoitei, N., Hoffmann, C.M., Ellegast, J.M., Ball, C.R., Obermayer, K., Gößele, U., Koch, B., Faber, K., Genze, F., Schrader, M., et al., 2012. Targeting of KRAS mutant tumors by HSP90 inhibitors involves degradation of STK33. J. Exp. Med. 209, 697–711.
Bastos, H., Lassalle, B., Chicheportiche, A., Riou, L., Testart, J., Allemand, I., Fouchet, P., 2005. Flow cytometric characterization of viable meiotic and postmeiotic cells by Hoechst 33342 in mouse spermatogenesis. Cytom. Part A 65, 40–49.
Bellvé, A.R., Cavicchia, J.C., Millette, C.F., O'Brien, D.A., Bhatnagar, Y.M., Dym, M., 1977. Spermatogenic cells of the prepuberal mouse. Isolation and morphological characterization. J. Cell Biol. 74, 68–85.
Borg, C.L., Wolski, K.M., Gibbs, G.M., O'Bryan, M.K., 2010. Phenotyping male infertility in the mouse: how to get the most out of a "non-performer. Hum. Reprod. Update 16, 205–224.
Brauksiepe, B., Mujica, A.O., Herrmann, H., Schmidt, E.R., 2008. The Serine/threonine kinase Stk33 exhibits autophosphorylation and phosphorylates the intermediate filament protein Vimentin. BMC Biochem. 9, 25.
Cole, A., Meistrich, M.L., Cherry, L.M., Trostle-Weige, P.K., 1988. Nuclear and manchette development in spermatids of normal and azh/azh mutant mice. Biol. Reprod. 38, 385–401.
Cooke, H.J., Saunders, P.T.K., 2002. Mouse models of male infertility. Nat. Rev. Genet. 3, 790–801.
Fliegauf, M., Benzing, T., Omran, H., 2007. When cilia go bad: cilia defects and ciliopathies. Nat. Rev. Mol. Cell Biol. 8, 880–893.
Hall, E.S., Eveleth, J., Boekelheide, K., 1991. 2,5-Hexanedione exposure alters the rat Sertoli cell cytoskeleton. II. Intermediate filaments and actin. Toxicol. Appl. Pharmacol. 111, 443–453.
Hermo, L., Pelletier, R.-M., Cyr, D.G., Smith, C.E., 2010. Surfing the wave, cycle, life history, and genes/proteins expressed by testicular germ cells. Part 1: background to spermatogenesis, spermatogonia, and spermatocytes. Microsc. Res. Tech. 73, 241–278.
Johnson, K.J., 2014. Testicular histopathology associated with disruption of the Sertoli cell cytoskeleton. Spermatogenesis 4, e979106.
Kleymenova, E., Swanson, C., Boekelheide, K., Gaido, K.W., 2005. Exposure in utero to di(n-butyl) phthalate alters the vimentin cytoskeleton of fetal rat Sertoli cells and disrupts Sertoli cell-gonocyte contact. Biol. Reprod. 73, 482–490.
Lehti, M.S., Sironen, A., 2016. Formation and function of the manchette and flagellum during spermatogenesis. Reproduction 151, R43–R54.
Lehti, M.S., Kotaja, N., Sironen, A., 2013. KIF3A is essential for sperm tail formation and manchette function. Mol. Cell. Endocrinol. 377, 44–55.
Liu, Y., DeBoer, K., de Kretser, D.M., O'Donnell, L., O'Connor, A.E., Merriner, D.J., Okuda, H., Whittle, B., Jans, D.A., Efthymiadis, A., et al., 2015. LRGUK-1 is required for basal body and manchette function during spermatogenesis and male fertility. PLoS Genet. 11, e1005090.
Matzuk, M.M., Lamb, D.J., 2008. The biology of infertility: research advances and clinical challenges. Nat. Med. 14, 1197–1213.
Mruk, D.D., Cheng, C.Y., 2004. Sertoli-sertoli and sertoli-germ cell interactions and their significance in germ cell movement in the seminiferous epithelium during spermatogenesis. Endocr. Rev. 25, 747–806.
Mujica, A.O., Hankeln, T., Schmidt, E.R., 2001. A novel serine/threonine kinase gene, STK33, on human chromosome 11p15.3. Gene 280, 175–181.
Mujica, A.O., Brauksiepe, B., Saaler-Reinhardt, S., Reuss, S., Schmidt, E.R., 2005. Differential expression pattern of the novel serine/threonine kinase, STK33, in mice and men. FEBS J. 272, 4884–4898.
Nebel, B.R., Amarose, A.P., Hackett, E.M., 1961. Calendar of gametogenic development in the prepuberal male mouse. Science 134, 832–833.
O'Donnell, L., O'Bryan, M.K., 2014. Microtubules and spermatogenesis. Semin. Cell Dev. Biol. 30, 45–54.
O'Donnell, L., Nicholls, P.K., O'Bryan, M.K., McLachlan, R.I., Stanton, P.G., 2011. Spermiation. Spermatogenesis 1, 14–35.
Petersen, C., Söder, O., 2006. The sertoli cell – a hormonal target and "super" nurse for germ cells that determines testicular size. Horm. Res. Paediatr. 66, 153–161.
Punab, M., Poolamets, O., Paju, P., Vihljajev, V., Pomm, K., Ladva, R., Korrovits, P., Laan, M., 2016. Causes of male infertility: a 9-year prospective monocentre study on 1737 patients with reduced total sperm counts STUDY QUESTION: what are the primary causes of severe male factor infertility? Hum. Reprod. 32, 18–31.
Reuss, S., Brauksiepe, B., Disque-Kaiser, U., Olivier, T., 2017. Serine/threonine-kinase 33 (Stk33) – Component of the neuroendocrine network? Brain Res. 1655, 152–160.
Scholl, C., Fröhling, S., Dunn, I.F., Schinzel, A.C., Barbie, D.A., Kim, S.Y., Silver, S.J., Tamayo, P., Wadlow, R.C., Ramaswamy, S., et al., 2009. Synthetic lethal interaction between oncogenic KRAS dependency and STK33 suppression in human cancer cells. Cell 137, 821–834.
Schultz, N., Hamra, F.K., Garbers, D.L., 2003. A multitude of genes expressed solely in meiotic or postmeiotic spermatogenic cells offers a myriad of contraceptive targets. Proc. Natl. Acad. Sci. USA 100, 12201–12206.
Sironen, A., Hansen, J., Thomsen, B., Andersson, M., Vilkki, J., Toppari, J., Kotaja, N., 2010. Expression of SPEF2 during mouse spermatogenesis and identification of IFT20 as an interacting protein. Biol. Reprod. 82, 580–590.
Turner, R.M., 2003. Tales from the tail: what do we really know about sperm motility? J. Androl. 24, 790–803.
Uhlen, M., Fagerberg, L., Hallstrom, B.M., Lindskog, C., Oksvold, P., Mardinoglu, A., Sivertsson, A., Kampf, C., Sjostedt, E., Asplund, A., et al., 2015. Tissue-based map of the human proteome. Science 347, 1260419.
W Chung, S.S., Choi ψ, C., Wang, X., Hallock, L., Wolgemuth, D.J., 2010. Aberrant distribution of junctional complex components in retinoic acid receptor alpha-deficient mice. Microsc. Res. Tech. 73, 583–596.
Yan, W., 2009. Male infertility caused by spermiogenic defects: lessons from gene knockouts. Mol. Cell. Endocrinol. 306, 24–32.
Yang, T., Song, B., Zhang, J., Yang, G.-S., Zhang, H., Yu, W.-F., Wu, M.-C., Lu, J.-H., Shen, F., 2016. STK33 promotes hepatocellular carcinoma through binding to c-Myc. Gut 65, 124–133.